Article

Enhanced critical current density in K-doped Ba122 polycrystalline bulk superconductors via fast densification

Fast densification of K-doped Ba122 bulks by spark plasma sintering

Improvement of critical current density achieving ~10^5 A/cm^2 at 5 K

Shinnosuke Tokuta, Yuta Hasegawa, Yusuke Shimada, Akiyasu Yamamoto

s195941r@st.go.tuat.ac.jp (S.T.)
akiyasu@cc.tuat.ac.jp (A.Y.)

Highlights

K-doped Ba122 polycrystalline bulks were synthesized via spark plasma sintering

Nearly single-phase and highly dense bulks were obtained in short period (5 min)

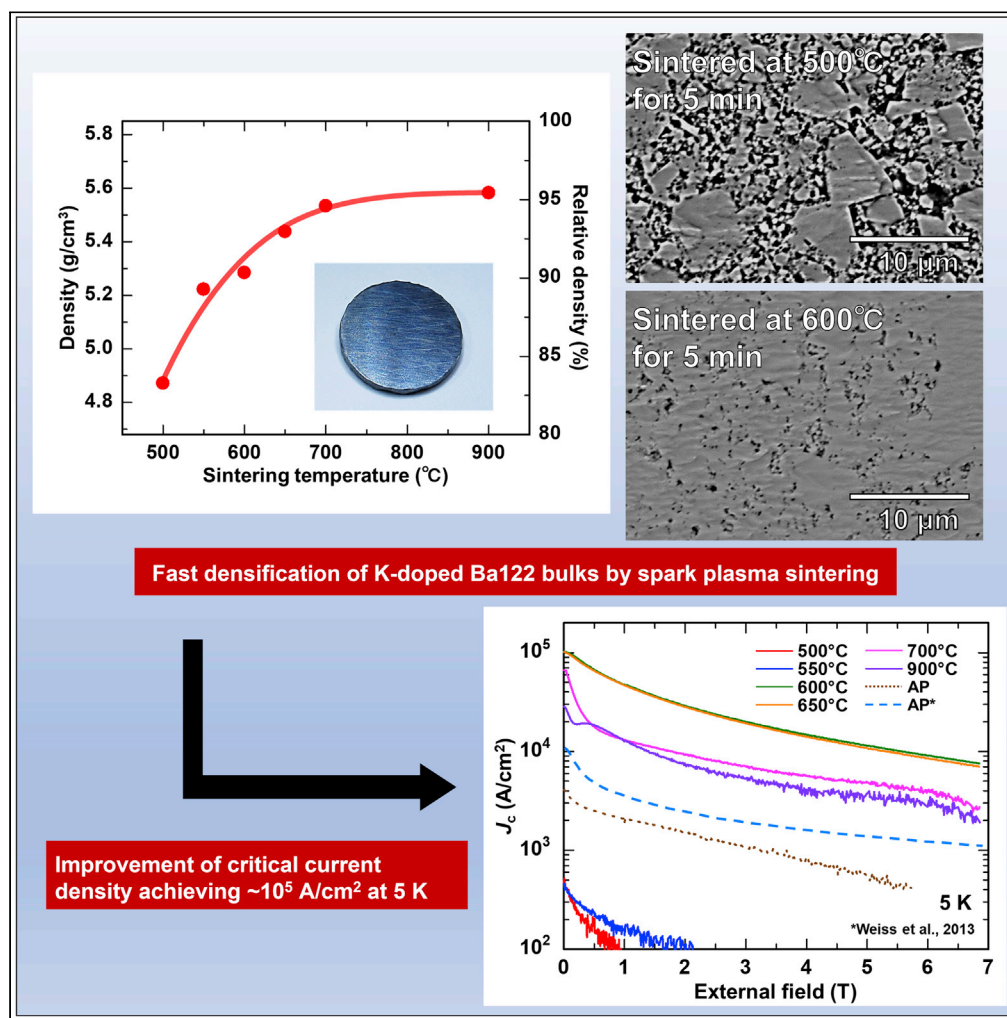The magnetic critical current density exceeded 10^5 A/cm^2 at 5 K

Article

Enhanced critical current density in K-doped Ba122 polycrystalline bulk superconductors via fast densification

Shinnosuke Tokuta,[1,*] Yuta Hasegawa,[1] Yusuke Shimada,[2] and Akiyasu Yamamoto[1,3,*]

SUMMARY

Iron-based superconductors are expected to be used in strong magnet applications owing to their excellent superconducting properties. The process of sintering a mechanically alloyed precursor powder is effective in achieving a high upper critical field and critical current density in $BaFe_2As_2$ (Ba122) polycrystalline bulk materials. However, when this process is applied to K-doped Ba122, which shows the highest critical temperature in the Ba122 family, suppressing the vaporization of potassium is challenging. In this study, spark plasma sintering (SPS) method was applied to K-doped Ba122 to achieve fast densification. In contrast to the conventional synthesis method, which requires several tens of hours, optimally K-doped bulks with near theoretical density were obtained after only 5 min of SPS, and the magnetic critical current density reached 10^5 A/cm^2 at 5 K. The demonstrated superconducting properties suggest that this fast densification technique is a useful tool for applying K-doped Ba122 to bulk trapped field magnets.

INTRODUCTION

As an iron-based superconductor (Hosono et al., 2018; Kamihara et al., 2008), $BaFe_2As_2$ (Ba122) (Rotter et al., 2008a, 2008b) is expected to be used in high magnetic field applications owing to its moderately high critical temperature (T_c) of ~38 K and high upper critical field (H_{c2}) of >50 T (Altarawneh et al., 2008; Tarantini et al., 2011). It exhibits a small electromagnetic anisotropy (γ) of 1–2 (Hänisch et al., 2015; Ishida et al., 2017; Tarantini et al., 2011; Vinod et al., 2011; Yamamoto et al., 2009; Yuan et al., 2009), a high irreversible field close to H_{c2} (Yamamoto et al., 2009), and a critical grain boundary angle (θ_c) of 5–9°, which is approximately twice that of yttrium barium copper oxide (Katase et al., 2011; Lee et al., 2009). These properties are advantageous for the application of Ba122 in polycrystalline forms and the fabrication of long wires and large bulks. Especially, Ba122 bulks are expected to be applied as powerful trapped field magnets (Weiss et al., 2015) for precision measuring instruments, levitation devices, and motors, taking advantage of their size proportional to the trapped magnetic field, which can be larger than that of REBCO, and their H_{c2}, which is higher than that of MgB_2.

Controlling the microstructure and improving the critical current density (J_c) are important for the application of iron-based superconductors. Generally, superconducting currents in polycrystalline superconductors are categorized into two types: intragranular currents, which flow within crystal grains without crossing the grain boundaries, and intergranular currents, which flow across the entire sample beyond the grain boundaries (Durrell et al., 2011; Hecher et al., 2016; Shimada et al., 2019; Yamamoto et al., 2008). The intergranular currents of Ba122 polycrystalline materials are considerably lower than the intragranular current of a Ba122 single crystal because of intrinsic weak-link, extrinsic structural defects, and compositional variations (Kametani et al., 2020). The J_c values of the intragranular currents of K-doped Ba122 single crystals and thin films are >10^6 A/cm^2 at 4 or 5 K under self-field conditions (Ishida et al., 2017; Qin et al., 2021), while those of the intergranular currents of K-doped Ba122 polycrystalline bulks synthesized under ambient pressure are ~10^4 A/cm^2 at 4.2 K under self-field conditions (Weiss et al., 2013).

The J_c value of K-doped Ba122 polycrystalline materials can be improved via high-pressure sintering. For example, polycrystalline bulks synthesized via hot isostatic pressing (HIP) achieve J_c values of ~1.2 × 10^5 (Weiss et al., 2013) and 2.3 × 10^5 A/cm^2 (Pak et al., 2020) at 4.2 K under self-field conditions, round wires

[1]Department of Applied Physics, Tokyo University of Agriculture and Technology, 2-24-16 Nacho, Koganei, Tokyo 184-8588, Japan
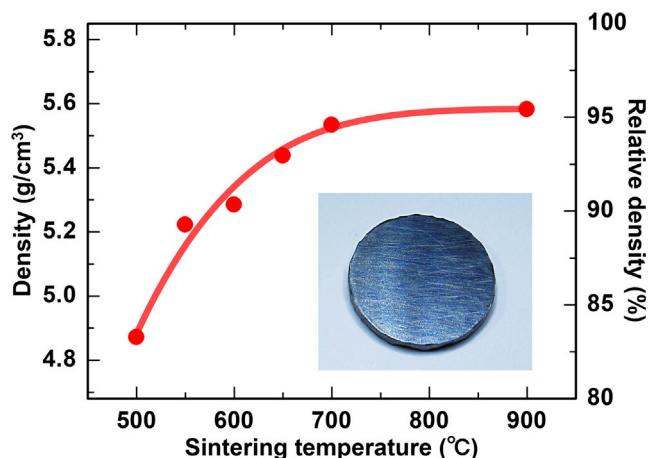
[2]IMR, Tohoku University, Sendai 980-8577, Japan

[3]Lead contact

*Correspondence:
s195941r@st.go.tuat.ac.jp (S.T.),
akiyasu@cc.tuat.ac.jp (A.Y.)
https://doi.org/10.1016/j.isci.2022.103992

Figure 1. Sintering temperature dependence of the density (left axis) and relative density to the theoretical density (right axis)
The inset presents an image of a bulk sample.

fabricated via HIP exhibit a J_c value of $\sim$3.8 $\times$ 10^4 A/cm^2 at 4.2 K and 10 T (Pyon et al., 2018), and tapes prepared via uniaxial hot pressing or HIP show a J_c value of >10^5 A/cm^2 at 4.2 K and 10 T (Huang et al., 2018; Liu et al., 2021; Yao and Ma, 2019). Previously, we improved the density and purity of Co-doped Ba122 polycrystalline bulks fabricated under ambient pressure using a mechanically alloyed precursor powder prepared via high-energy ball milling. At 5 K under self-field conditions, the J_c value of these bulks improved to a value approximately three times that reported in a previous study (Tokuta et al., 2020). Furthermore, the H_{c2} value of Co-doped Ba122 polycrystalline bulks can be artificially enhanced and adjusted by introducing lattice defects into the grains via high-energy ball milling (Tokuta and Yamamoto, 2019).

In many cases, the high-pressure sintering of Ba122 has been carried out in a powder-in-tube (PIT) condition. This is advantageous for improving the mechanical properties of wires and for suppressing the vaporization of potassium, which has a high equilibrium vapor pressure, but PIT is less suitable for the preparation of large bulks.

In this study, K-doped Ba122 polycrystalline bulks were synthesized via spark plasma sintering (SPS), a pressure-assisted sintering method expected to achieve fast densification, using a mechanically alloyed precursor powder prepared via high-energy ball milling (Maltsev et al., 2019; Pervakov and Vlasenko, 2020; Tokuta et al., 2020; Tokuta and Yamamoto, 2019; Weiss et al., 2013). The density, microstructure, phase composition, and superconducting properties of the fabricated bulk samples were evaluated as a function of the sintering temperature. After sintering at 600°C and 650°C for 5 min, nearly single-phase bulks with a high density of >90% and a J_c value exceeding 10^5 A/cm^2 at 5 K under self-field conditions were obtained; this J_c value was one order of magnitude higher than that of polycrystalline bulks synthesized under ambient pressure.

RESULTS AND DISCUSSION

Density and microstructure

Figure 1 presents the sintering temperature dependence of the density and relative density to the theoretical density for K40%-doped Ba122 (5.85 g/cm^3). The theoretical density was calculated using the lattice parameter values of a K40%-doped Ba122 single crystal from the literature (a = 3.912 Å and c = 13.33 Å (Rotter et al., 2008a; Zaikina et al., 2014)). The density increased with increasing sintering temperature, and a high relative density of >90% was obtained for the samples sintered at >600°C, reaching 95.4% for the sample sintered at 900°C. For reference, the relative densities of other iron-based superconducting bulks synthesized via SPS were $\sim$80% for Co-doped Ba122 (Zaikina et al., 2018), 96% for NdFeAsO$_{0.75}$F$_{0.25}$ (Kursumovic et al., 2010), 90% for FeSe$_{0.5}$Te$_{0.5}$ (Puneet et al., 2015), and 96.2% for CaKFe$_4$As$_4$ (Ishida et al., 2020). Figure 2 shows the backscattered electron images of the samples sintered at (a) 500°C, (b) 600°C, and (c) 900°C. The sample sintered at 500°C (Figure 2A) showed continuous voids, and the void area fraction was larger than those of the other samples, suggesting poor connectivity. The sample sintered at
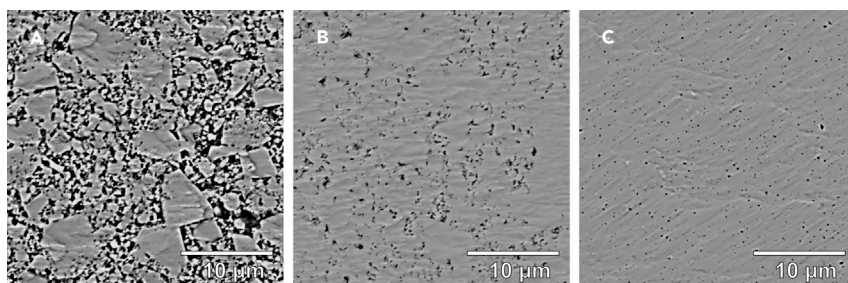
Figure 2. SEM images of the samples
Backscattered electron images of polished cross-sectional surfaces of the samples sintered at (A) 500°C, (B) 600°C, and (C) 900°C.
The gray and black contrasts correspond to the K-doped $BaFe_2As_2$ (Ba122) phase and voids, respectively.

600°C (Figure 2B) presented isolated voids and reduced void area fraction, indicating improved connectivity. In the sample sintered at 900°C (Figure 2C), the void area fraction further decreased and small round-shaped pores were observed. The microstructures shown in Figures 2A–2C were assumed to correspond to the early, middle, and end stages of sintering, respectively, consistent with the increase in the density with increasing sintering temperature (Figure 1). The density of the K40%-doped Ba122 polycrystalline sample prepared under ambient pressure was ~4 g/cm^3 (~68%) (Weiss et al., 2013). It is noteworthy that high-density samples were obtained after only 5 min of sintering at >600°C, possibly because of porosity reduction owing to the pressure, heating from inside and outside the sample (self-heating by Joule heating and heat transfer from the mold, respectively), and electric field diffusion effect (Cavaliere et al., 2019; Tokita, 2021).

Constituent phases and structural properties

Figure 3 shows the XRD patterns of the surfaces of the bulk samples. Ba122 was obtained as the main phase in all samples. FeAs impurity peaks were observed in the samples sintered at 500°C, 550°C, and 700°C, and nearly single-phase Ba122 was obtained in the samples sintered at 600°C, 650°C, and 900°C. The full width at the half maximum of the main (103) peak of the Ba122 phase gradually decreased from 0.66° for the sample sintered at 500°C to 0.38° for that sintered at 650°C and suddenly decreased to 0.19° for those sintered at 700°C and 900°C. This suggests that the crystallinity improved with increasing sintering temperature and the grain size increased because of grain growth at >700°C. As the sintering temperature increased from 500°C to 900°C, the relative intensity of the (200) peak decreased from 29.2% to 15.3% and that of the (002) peak increased from 13.5% to 21.4%, suggesting the occurrence of weak texturing or the increase in area of ab plane by anisotropic grain growth in the samples sintered at high temperatures. The lattice parameters (a and c) of the samples are shown in Table 1. A slight increase in the a-axis length and decrease in the c-axis length were observed with increasing sintering temperature. The relations between the lattice parameters of a $Ba_{1-x}K_xFe_2As_2$ single crystal (Rotter et al., 2008a; Zaikina et al., 2014) and the K-doping level of the Ba site (x) are $x_a = -8.246a + 32.66$ and $x_c = 1.194c - 15.52$. The K-doping levels of the samples estimated from the lattice parameters (x_a and x_c) and measured by EDX (x_{EDX}) are also shown in Table 1. Based on the lattice parameters, we estimate that the K-doping levels of the samples sintered at 600°C and 650°C, which showed nearly single phase, were ~42%. Note that x_a and x_c are rough estimations because lattice parameters of the samples prepared via high-energy ball milling are affected by lattice defects (Tokuta and Yamamoto, 2019). Based on the EDX, the K-doping levels of the samples sintered at 600°C, 700°C, and 900°C were ~38%, which is close to the nominal composition. These suggest that the vaporization of potassium during sintering was insignificant.

Electrical resistivity and critical temperature

Figure 4 shows the temperature dependence of the electrical resistivity (ρ) normalized by ρ at 300 K, and the inset presents the temperature dependence of ρ near T_c normalized by ρ at 40 K. The electrical resistivities of all samples decreased with decreasing temperature, showing superconducting transition and zero resistance. Figure 5 shows the sintering temperature dependence of T_c and T_c^{zero}. T_c increased monotonically with increasing sintering temperature owing to the improvement of crystallinity from 33.1 K for the sample sintered at 500°C to 37.8 K for the sample sintered at 900°C, which is comparable to that of single crystals (Rotter et al., 2008b). The lower T_c of the samples sintered at lower temperature is possibly due to the low crystallinity caused by the introduction of the lattice defects via high-energy ball milling (Tokuta and
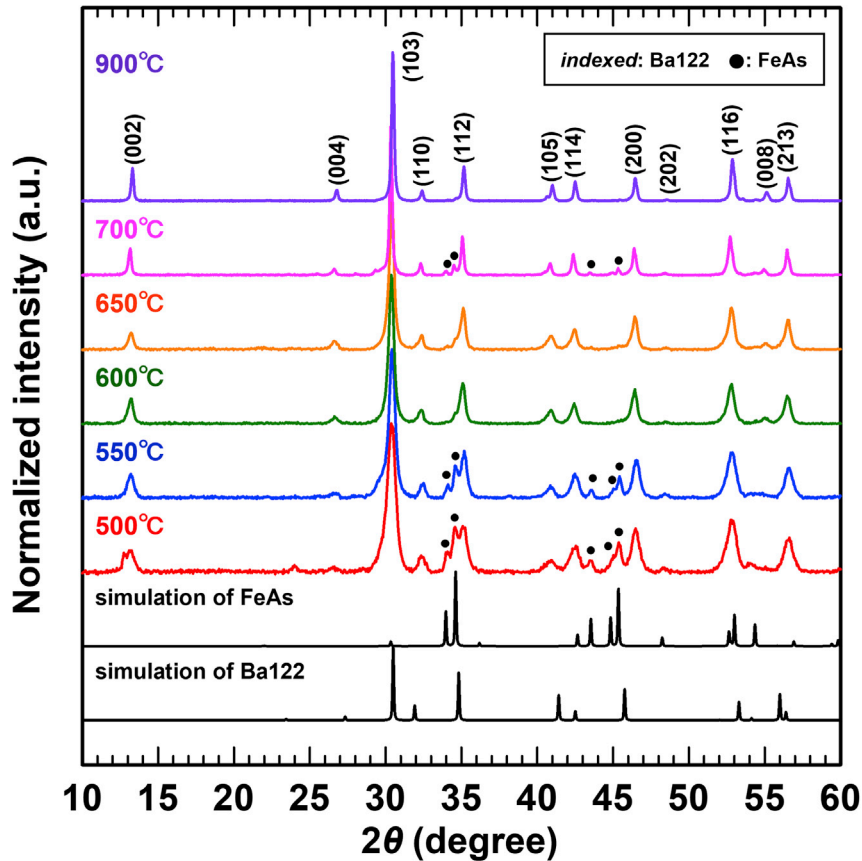
Figure 3. X-ray diffraction patterns of the surfaces of the bulk samples
The intensity of each sample is normalized by the intensity of the (103) peak of that sample, and the offset is corrected.

Yamamoto, 2019). Furthermore, T_c^{zero} increased monotonically with increasing sintering temperature and the superconducting transition width ($T_c - T_c^{zero}$) sharpened considerably from 12.4 K for the sample sintered at 500°C to 1.2 K for the sample sintered at 900°C. The residual resistivity ratio ($RRR = \rho$ (300 K)/ρ (40 K)) increased with the sintering temperature, and the samples sintered at 500°C, 550°C, 600°C, 650°C, 700°C, and 900°C showed the RRR values of 2.22, 3.23, 4.25, 4.91, 6.79, and 7.95, respectively. The RRR values reported in the literature are 4.59 (Chen et al., 2009), 5.55 (Rotter et al., 2008b), 6.97 (Mu et al., 2009), 7.06 (Luo et al., 2008), and 9.94 (Nakajima et al., 2015) for single crystals (in-plane), 6.80 (Qin et al., 2021) for thin films (in-plane), and 5.00 (Liu et al., 2019) and 6.58 (Weiss et al., 2012) for polycrystalline materials. The RRR value of the sample sintered at >700°C is equivalent to those of single crystals and thin films and higher than those of polycrystalline materials. A double superconducting transition was observed in the samples sintered at 500°C, 550°C, 600°C, and 650°C but not in the samples sintered at 700°C and 900°C. The transitions observed at higher and lower temperatures were assumed to correspond to those

Table 1. The lattice parameters (*a* and *c*) of the samples and the K-doping levels estimated from the lattice parameters (x_a and x_c) and measured by EDX (x_{EDX})

Sintering temperature (°C)	*a* (Å)	*c* (Å)	x_a	x_c	x_{EDX}
500	3.9023	13.3678	0.481	0.441	–
550	3.9031	13.3850	0.474	0.462	–
600	3.9100	13.3464	0.418	0.416	0.380
700	3.9093	13.3465	0.424	0.416	–
800	3.9074	13.3576	0.439	0.429	0.378
900	3.9109	13.3309	0.410	0.397	0.384
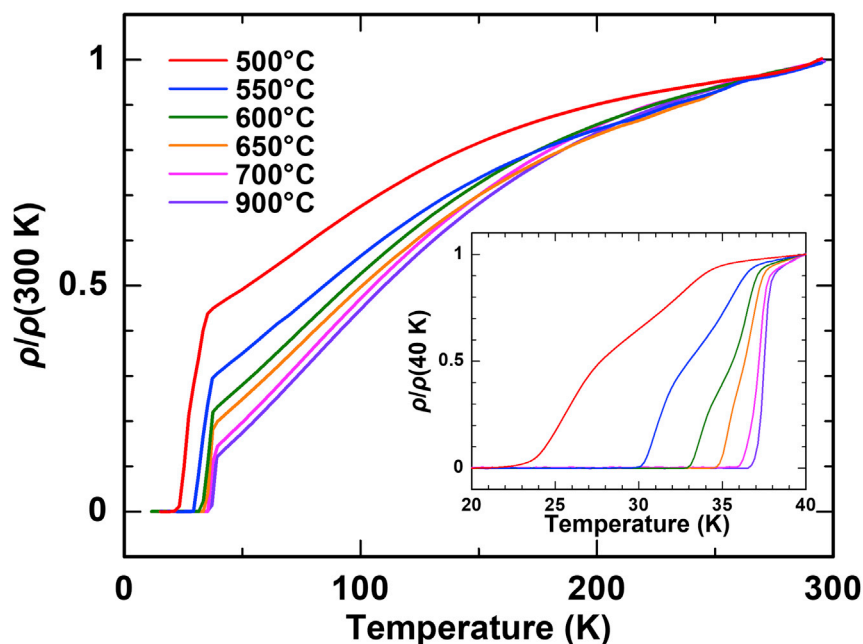
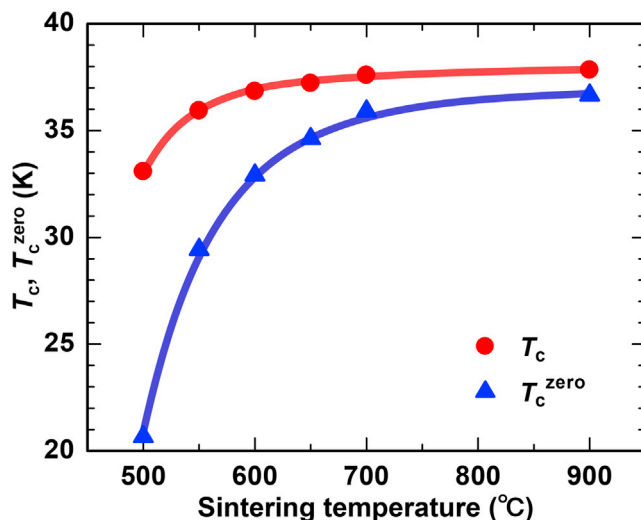**Figure 4. Temperature dependence of the electrical resistivity (ρ) normalized by ρ at 300 K**
The inset shows the temperature dependence of ρ normalized by ρ at 40 K.

of grains and grain boundaries, respectively, analogous to those observed for cuprates (Cai et al., 1998). These transport measurements suggest that electrically well-connected samples could be obtained by sintering at >700°C.

Magnetization and critical current density

Figures 6 and 7 plot the magnetic hysteresis loops and the external field dependences of J_c, respectively, for the various samples at 5 K. The samples sintered at 500°C and 550°C exhibited almost no magnetic hysteresis and a very small J_c values of <10^3 A/cm^2. This may be attributed to large amounts of impurities, poor connectivity, and low T_c. The samples sintered at 600°C and 650°C, in which the purity, connectivity, and T_c were improved, showed high symmetric magnetic hysteresis loops and a high J_c values of ~1.0 × 10^5 A/cm^2 under


Figure 5. Sintering temperature dependence of the critical temperature (T_c) and zero resistance temperature (T_c^{zero})
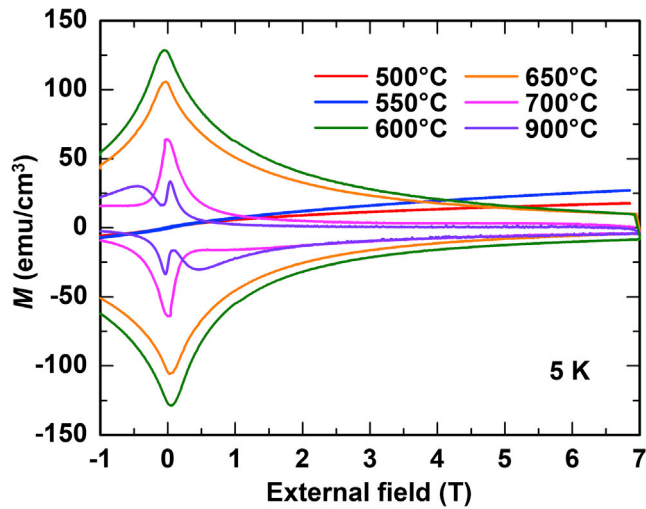
**Figure 6. Magnetic hysteresis loops of various samples at 5 K**

self-field conditions. This J_c value is an order of magnitude higher than those of K-doped Ba122 polycrystalline bulks synthesized under ambient pressure (Weiss et al., 2013) and comparable to those of polycrystalline bulks prepared via HIP (Pak et al., 2020; Weiss et al., 2013). Remanent magnetization measurement (Yamamoto et al., 2008) indicates that the J_c's of the samples sintered at 600°C and 650°C mostly reflect intergranular currents. The magnetic hysteresis loop of the sample sintered at 700°C was less symmetric, and broad secondary peaks appeared at approximately ± 0.5 T in the magnetic hysteresis loop of the sample sintered at 900°C. Although the density and T_c of the samples sintered at 700°C and 900°C were higher than those of the samples sintered at 600°C and 650°C, their J_c values under self-field conditions decreased to 6.7×10^4 and 2.9×10^4 A/cm^2, respectively.

A possible reason for the decrease in the J_c values of the samples sintered at 700°C and 900°C is the increase in their grain sizes. Figures 8A and 8B present a low-angle annular dark-field STEM (LAADF-STEM) image and electron diffraction image of the sample sintered at 700°C, while Figures 8C–8H depict elemental mapping images of the same sample. The spots in the electron diffraction image are seen in various directions, implying that the sample showed a nearly random orientation. The elemental mapping images revealed the ~100 nm FeAs phase. The grain sizes of the samples sintered at 600°C, 700°C, and 900°C were <50 nm, 0.1–0.5 μm, and
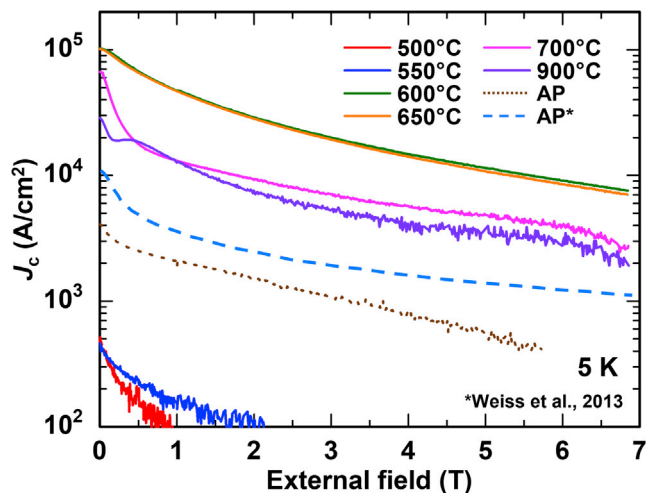
Figure 7. External field dependence of the magnetic critical current density (J_c) for various samples at 5 K
The dotted and dashed lines indicate data for K40%-doped Ba122 polycrystalline bulks synthesized under ambient pressure (AP) in this study and reported in Weiss et al. (Weiss et al., 2013), respectively.
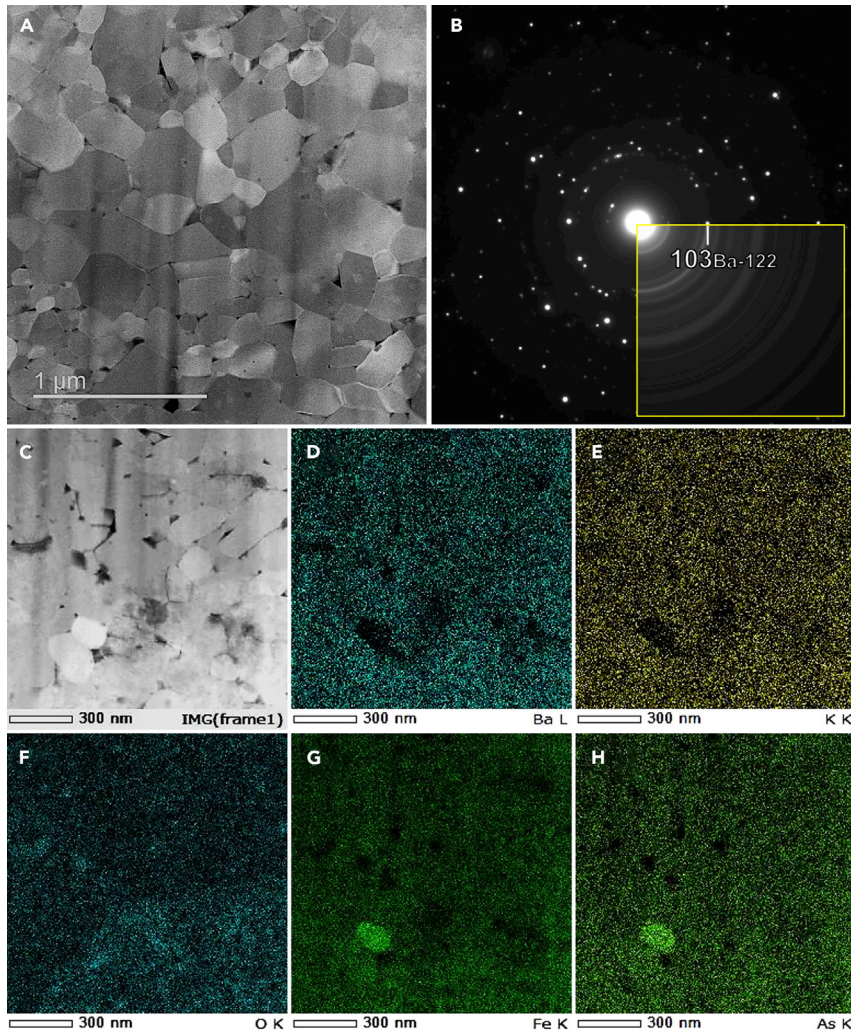
Figure 8. STEM and EDX images of the sample sintered at 700°C
(A) Low-angle annular dark-field scanning transmission electron microscopy image, (B) electron diffraction image, and (C–H) elemental mapping images of polished cross-sectional surface.

0.3–3 μm, respectively, indicating a considerable increase of grain size with increasing sintering temperature. Hecher et al. reported that, because the grain boundary of Ba122 presents a Josephson junction, the J_c value of the intergranular currents decrease as the grain size and junction area increase (Hecher et al., 2016). In such polycrystalline samples, the magnetic hysteresis loop exhibits two types of peaks by the contribution of inter-granular and intragranular currents; this is consistent with the shape of the magnetic hysteresis loop of the sample sintered at 900°C (Figure 6). Moreover, Shimada et al. experimentally showed that the J_c value of the intergranular current increases with decreasing grain size for Co-doped Ba122 polycrystalline bulks (Shimada et al., 2019). The sintering temperatures of 600°C and 650°C, at which the highest J_c values were obtained herein, were well balanced between the enhancement of T_c and the J_c values of the intra and inter-granular currents owing to improved purity, crystallinity, and grain bonding and the decrease of J_c value of the intergranular current resulting from grain growth. However, because the electrical resistivity of the samples sintered at 600°C and 650°C shown in the inset of Figure 4 exhibited a double transition, the preparation conditions of the precursor powder and the SPS conditions can be improved.

Conclusions

K-doped Ba122 polycrystalline bulks were prepared using the SPS method. High-purity samples with a high relative density of 90% were obtained after 5 min of sintering at >600°C. Nearly single-phase

and optimal-doped Ba122 was obtained for the samples sintered at 600°C and 650°C. As the sintering temperature increased, the grain crystallinity and connectivity improved and both T_c and T_c^{zero} improved. A high J_c values of $>10^5$ A/cm^2 were obtained at 5 K under self-field conditions for the samples sintered at 600°C and 650°C, while the J_c values decreased for the samples sintered at >700°C, likely due to the increased grain size. SPS is a promising method for synthesizing Ba122 polycrystalline bulks for practical use because it is a fast densification technique and suitable for the fabrication of large disk-shaped bulks.

Limitations of the study

Although J_c of a K-doped Ba122 polycrystalline bulk was improved by investigating the effects of the sintering temperature of SPS in this work, there are many other synthesis conditions that may affect J_c, such as dwell time, applied pressure, and the condition of the precursor powder. These need to be investigated, and the bulk size also needs to be increased for bulk magnet applications.

STAR★METHODS

Detailed methods are provided in the online version of this paper and include the following:

- KEY RESOURCES TABLE
- RESOURCE AVAILABILITY
  ○ Lead contact
  ○ Materials availability
  ○ Data and code availability
- METHOD DETAILS
  ○ Sample preparation
  ○ Evaluations

AUTHOR CONTRIBUTIONS

Conceptualization, S.T. and A.Y.; Methodology, S.T.; Investigation, S.T and Y.S; Writing – Original Draft, S.T.; Writing –Review & Editing, S.T., Y.H., Y.S., and A.Y.; Supervision, A.Y.

DECLARATION OF INTERESTS

The authors declare no competing interests.

REFERENCES

Altarawneh, M.M., Collar, K., Mielke, C.H., Ni, N., Bud'Ko, S.L., and Canfield, P.C. (2008). Determination of anisotropic H_{c2} up to 60 T in Ba$_{0.55}$K$_{0.45}$Fe$_2$As$_2$ single crystals. Phys. Rev. B *78*, 220505. https://doi.org/10.1103/PhysRevB.78.220505.

Cai, X.Y., Polyanskii, A., Li, Q., Riley, G.N., and Larbalestier, D.C. (1998). Current-limiting mechanisms in individual filaments extracted from superconducting tapes. Nature *392*, 906–909. https://doi.org/10.1038/31907.

Cavaliere, P., Sadeghi, B., and Shabani, A. (2019). Spark plasma sintering: process fundamentals. In Spark Plasma Sintering of Materials, P. Cavaliere, ed. (Springer International Publishing), pp. 3–20. https://doi.org/10.1007/978-3-030-05327-7_1.

Chen, H., Ren, Y., Qiu, Y., Bao, W., Liu, R.H., Wu, G., Wu, T., Xie, Y.L., Wang, X.F., Huang, Q., and Chen, X.H. (2009). Coexistence of the spin-density wave and superconductivity in Ba$_{1−x}$K$_x$Fe$_2$As$_2$. EPL *85*, 17006. https://doi.org/10.1209/0295-5075/85/17006.

Durrell, J.H., Eom, C.B., Gurevich, A., Hellstrom, E.E., Tarantini, C., Yamamoto, A., and Larbalestier, D.C. (2011). The behavior of grain boundaries in the Fe-based superconductors. Rep. Prog. Phys. *74*, 124511. https://doi.org/10.1088/0034-4885/74/12/124511.

Hänisch, J., Iida, K., Kurth, F., Reich, E., Tarantini, C., Jaroszynski, J., Förster, T., Fuchs, G., Hühne, R., Grinenko, V., et al. (2015). High field superconducting properties of Ba(Fe$_{1−x}$Co$_x$)$_2$As$_2$

thin films. Sci. Rep. *5*, 17363. https://doi.org/10.1038/srep17363.

Häßler, W., Hermann, H., Herrmann, M., Rodig, C., Aubele, A., Schmolinga, L., Sailer, B., and Holzapfel, B. (2013). Influence of the milling energy transferred to the precursor powder on the microstructure and the superconducting properties of MgB_2 wires. Supercond. Sci. Technol. *26*, 025005. https://doi.org/10.1088/0953-2048/26/2/025005.

Hecher, J., Baumgartner, T., Weiss, J.D., Tarantini, C., Yamamoto, A., Jiang, J., Hellstrom, E.E., Larbalestier, D.C., and Eisterer, M. (2016). Small grains: a key to high-field applications of granular Ba-122 superconductors? Supercond. Sci. Technol. *29*, 025004. https://doi.org/10.1088/0953-2048/29/2/025004.

Hosono, H., Yamamoto, A., Hiramatsu, H., and Ma, Y. (2018). Recent advances in iron-based superconductors toward applications. Mater. Today *21*, 278–302. https://doi.org/10.1016/j.mattod.2017.09.006.

Huang, H., Yao, C., Dong, C., Zhang, X., Wang, D., Cheng, Z., Li, J., Awaji, S., Wen, H., and Ma, Y. (2018). High transport current superconductivity in powder-in-tube $Ba_{0.6}K_{0.4}Fe_2As_2$ tapes at 27 T. Supercond. Sci. Technol. *31*, 015017. https://doi.org/10.1088/1361-6668/aa9912.

Ishida, S., Pavan Kumar Naik, S., Tsuchiya, Y., Mawatari, Y., Yoshida, Y., Iyo, A., Eisaki, H., Kamiya, Y., Kawashima, K., and Ogino, H. (2020). Synthesis of $CaKFe_4As_4$ bulk samples with high critical current density using a spark plasma sintering technique. Supercond. Sci. Technol. *33*, 094005. https://doi.org/10.1088/1361-6668/aba019.

Ishida, S., Song, D., Ogino, H., Iyo, A., Eisaki, H., Nakajima, M., Shimoyama, J., and Eisterer, M. (2017). Doping-dependent critical current properties in K, Co, and P-doped $BaFe_2As_2$ single crystals. Phys. Rev. B *95*, 014517. https://doi.org/10.1103/PhysRevB.95.014517.

Kametani, F., Su, Y.F., Collantes, Y., Pak, C., Tarantini, C., Larbalestier, D., and Hellstrom, E. (2020). Chemically degraded grain boundaries in fine-grain $Ba_{0.6}K_{0.4}Fe_2As_2$ polycrystalline bulks. Appl. Phys. Express *13*. https://doi.org/10.35848/1882-0786/abbfdf.

Kamihara, Y., Watanabe, T., Hirano, M., and Hosono, H. (2008). Iron-based layered superconductor $La[O_{1-x}F_x]FeAs$ (x = 0.05−0.12) with T_c = 26 K. J. Am. Chem. Soc. *130*, 3296–3297. https://doi.org/10.1021/ja800073m.

Katase, T., Ishimaru, Y., Tsukamoto, A., Hiramatsu, H., Kamiya, T., Tanabe, K., and Hosono, H. (2011). Advantageous grain boundaries in iron pnictide superconductors. Nat. Commun. *2*, 409. https://doi.org/10.1038/ncomms1419.

Kursumovic, A., Durrell, J.H., Chen, S.K., and MacManus-Driscoll, J.L. (2010). Ambient/low pressure synthesis and fast densification to achieve 55 K T_c superconductivity in $NdFeAsO_{0.75}F_{0.25}$. Supercond. Sci. Technol. *23*, 025022. https://doi.org/10.1088/0953-2048/23/2/025022.

Lee, S., Jiang, J., Weiss, J.D., Folkman, C.M., Bark, C.W., Tarantini, C., Xu, A., Abraimov, D.,

Polyanskii, A., Nelson, C.T., et al. (2009). Weak-link behavior of grain boundaries in superconducting $Ba(Fe_{1-x}Co_x)_2As_2$ bicrystals. Appl. Phys. Lett. *95*, 212505. https://doi.org/10.1063/1.3262953.

Liu, S., Cheng, Z., Yao, C., Dong, C., Wang, D., Huang, H., Li, L., Xu, G., Zhu, Y., Liu, F., et al. (2019). High critical current density in Cu/Ag composited sheathed $Ba_{0.6}K_{0.4}Fe_2As_2$ tapes prepared by hot isostatic pressing. Supercond. Sci. Technol. *32*, 044007. https://doi.org/10.1088/1361-6668/aaff27.

Liu, S., Yao, C., Huang, H., Dong, C., Guo, W., Cheng, Z., Zhu, Y., Awaji, S., and Ma, Y. (2021). High- performance $Ba_{1-x}K_xFe_2As_2$ superconducting tapes with grain texture engineered via a scalable fabrication. Sci. China Mater. *64*, 2530. https://doi.org/10.1007/s40843-020-1643-1.

Luo, H., Wang, Z., Yang, H., Cheng, P., Zhu, X., and Wen, H.H. (2008). Growth and characterization of $A_{1-x}K_xFe_2As_2$ (A = Ba, Sr) single crystals with x = 0–0.4. Supercond. Sci. Technol. *21*, 125014. https://doi.org/10.1088/0953-2048/21/12/125014.

Maltsev, E.I., Pervakov, K.S., and Vlasenko, V.A. (2019). Synthesis of iron-based superconductor $Ba_{0.6}K_{0.4}Fe_2As_2$ by mechanical alloying. Bull. Lebedev Phys. Inst. *46*, 248–250. https://doi.org/10.3103/S1068335619080025.

Mu, G., Luo, H., Wang, Z., Shan, L., Ren, C., and Wen, H.H. (2009). Low temperature specific heat of the hole-doped $Ba_{0.6}K_{0.4}Fe_2As_2$ single crystals. Phys. Rev. B *79*, 174501. https://doi.org/10.1103/PhysRevB.79.174501.

Nakajima, M., Ishida, S., Tanaka, T., Kihou, K., Tomioka, Y., Saito, T., Lee, C.H., Fukazawa, H., Kohori, Y., Kakeshita, T., et al. (2015). Normal-state charge dynamics in doped $BaFe_2As_2$: roles of doping and necessary ingredients for superconductivity. Sci. Rep. *4*, 5873. https://doi.org/10.1038/srep05873.

Pak, C., Su, Y.F., Collantes, Y., Tarantini, C., Hellstrom, E.E., Larbalestier, D.C., and Kametani, F. (2020). Synthesis routes to eliminate oxide impurity segregation and their influence on intergrain connectivity in K-doped $BaFe_2As_2$ polycrystalline bulks. Supercond. Sci. Technol. *33*, 084010. https://doi.org/10.1088/1361-6668/aba01a.

Pervakov, K.S., and Vlasenko, V.A. (2020). Synthesis of electron- and hole-doped bulk $BaFe_2As_2$ superconductors by mechanical alloying. Ceram. Int. *46*, 8625–8630. https://doi.org/10.1016/j.ceramint.2019.12.095.

Puneet, P., Podila, R., He, J., Rao, A.M., Howard, A., Cornell, N., and Zakhidov, A.A. (2015). Synthesis and superconductivity in spark plasma sintered pristine and graphene-doped $FeSe_{0.5}Te_{0.5}$. Nanotechnol. Rev. *4*, 411–417. https://doi.org/10.1515/ntrev-2015-0018.

Pyon, S., Suwa, T., Tamegai, T., Takano, K., Kajitani, H., Koizumi, N., Awaji, S., Zhou, N., and Shi, Z. (2018). Improvements of fabrication processes and enhancement of critical current densities in $(Ba,K)Fe_2As_2$ HIP wires and tapes. Supercond. Sci. Technol. *31*, 055016. https://doi.org/10.1088/1361-6668/aab8c3.

Qin, D., Iida, K., Hatano, T., Saito, H., Ma, Y., Wang, C., Hata, S., Naito, M., and Yamamoto, A. (2021). Realization of epitaxial thin films of the superconductor K-doped $BaFe_2As_2$. Phys. Rev. Mater. *5*, 014801. https://doi.org/10.1103/PhysRevMaterials.5.014801.

Rotter, M., Pangerl, M., Tegel, M., and Johrendt, D. (2008a). Superconductivity and crystal structures of $(Ba_{1-x}K_x)Fe_2As_2$ (x = 0–1). Angew. Chem. Int. Ed. *47*, 7949–7952. https://doi.org/10.1002/anie.200803641.

Rotter, M., Tegel, M., and Johrendt, D. (2008b). Superconductivity at 38 K in the iron arsenide $(Ba_{1-x}K_x)Fe_2As_2$. Phys. Rev. Lett. *101*, 107006. https://doi.org/10.1103/PhysRevLett.101.107006.

Shimada, Y., Yamamoto, A., Hayashi, Y., Kishio, K., Shimoyama, J., Hata, S., and Konno, T.J. (2019). The formation of defects and their influence on inter- and intra-granular current in sintered polycrystalline 122 phase Fe-based superconductors. Supercond. Sci. Technol. *32*, 084003. https://doi.org/10.1088/1361-6668/ab0eb6.

Tarantini, C., Gurevich, A., Jaroszynski, J., Balakirev, F., Bellingeri, E., Pallecchi, I., Ferdeghini, C., Shen, B., Wen, H.H., and Larbalestier, D.C. (2011). Significant enhancement of upper critical fields by doping and strain in iron-based superconductors. Phys. Rev. B *84*, 184522. https://doi.org/10.1103/PhysRevB.84.184522.

Tokita, M. (2021). Progress of spark plasma sintering (SPS) method, systems, ceramics applications and industrialization. Ceramics *4*, 160–198. https://doi.org/10.3390/ceramics4020014.

Tokuta, S., Shimada, Y., and Yamamoto, A. (2020). Evolution of intergranular microstructure and critical current properties of polycrystalline Co-doped $BaFe_2As_2$ through high-energy milling. Supercond. Sci. Technol. *33*, 094010. https://doi.org/10.1088/1361-6668/aba545.

Tokuta, S., and Yamamoto, A. (2019). Enhanced upper critical field in Co-doped Ba122 superconductors by lattice defect tuning. APL Mater. *7*, 111107. https://doi.org/10.1063/1.5098057.

Vinod, K., Satya, A.T., Sharma, S., Sundar, C.S., and Bharathi, A. (2011). Upper critical field anisotropy in $BaFe_{2-x}Co_xAs_2$ single crystals synthesized without flux. Phys. Rev. B *84*, 012502. https://doi.org/10.1103/PhysRevB.84.012502.

Weiss, J.D., Jiang, J., Polyanskii, A.A., and Hellstrom, E.E. (2013). Mechanochemical synthesis of pnictide compounds and superconducting $Ba_{0.6}K_{0.4}Fe_2As_2$ bulks with high critical current density. Supercond. Sci. Technol. *26*, 074003. https://doi.org/10.1088/0953-2048/26/7/074003.

Weiss, J.D., Tarantini, C., Jiang, J., Kametani, F., Polyanskii, A.A., Larbalestier, D.C., and Hellstrom, E.E. (2012). High intergrain critical current density in fine-grain $(Ba_{0.6}K_{0.4})Fe_2As_2$ wires and bulks. Nat. Mater. *11*, 682–685. https://doi.org/10.1038/nmat3333.

Weiss, J.D., Yamamoto, A., Polyanskii, A.A., Richardson, R.B., Larbalestier, D.C., and Hellstrom, E.E. (2015). Demonstration of an

iron-pnictide bulk superconducting magnet capable of trapping over 1 T. Supercond. Sci. Technol. *28*, 112001. https://doi.org/10.1088/0953-2048/28/11/112001.

Yamamoto, A., Jaroszynski, J., Tarantini, C., Balicas, L., Jiang, J., Gurevich, A., Larbalestier, D.C., Jin, R., Sefat, A.S., McGuire, M.A., et al. (2009). Small anisotropy, weak thermal fluctuations, and high field superconductivity in Co-doped iron pnictide Ba(Fe$_{1-x}$Co$_x$)$_2$As$_2$. Appl. Phys. Lett. *94*, 062511. https://doi.org/10.1063/1.3081455.

Yamamoto, A., Polyanskii, A.A., Jiang, J., Kametani, F., Tarantini, C., Hunte, F., Jaroszynski, J., Hellstrom, E.E., Lee, P.J., Gurevich, A., et al. (2008). Evidence for two distinct scales of current flow in polycrystalline Sm and Nd iron oxypnictides. Supercond. Sci. Technol. *21*, 095008. https://doi.org/10.1088/0953-2048/21/9/095008.

Yao, C., and Ma, Y. (2019). Recent breakthrough development in iron-based superconducting wires for practical applications. Supercond. Sci. Technol. *32*, 023002. https://doi.org/10.1088/1361-6668/aaf351.

Yuan, H.Q., Singleton, J., Balakirev, F.F., Baily, S.A., Chen, G.F., Luo, J.L., and Wang, N.L. (2009). Nearly isotropic superconductivity in (Ba,K)Fe$_2$As$_2$. Nature *457*, 565–568. https://doi.org/10.1038/nature07676.

Zaikina, J.V., Batuk, M., Abakumov, A.M., Navrotsky, A., and Kauzlarich, S.M. (2014). Facile synthesis of Ba$_{1-x}$K$_x$Fe$_2$As$_2$ superconductors via hydride route. J. Am. Chem. Soc. *136*, 16932–16939. https://doi.org/10.1021/ja509907r.

Zaikina, J.V., Kwong, M.Y., Baccam, B., and Kauzlarich, S.M. (2018). Superconductor-in-an-hour: spark plasma synthesis of Co- and Ni-doped BaFe$_2$As$_2$. Chem. Mater. *30*, 8883–8890. https://doi.org/10.1021/acs.chemmater.8b04039.

STAR★METHODS

KEY RESOURCES TABLE

REAGENT or RESOURCE	SOURCE	IDENTIFIER
Chemicals, peptides, and recombinant proteins		
Barium (Ba)	Furuuchi Chemical Co., Ltd.	CAS: 7440-39-3
Potassium (K)	Acros Organics BVBA	CAS: 7440-09-7
Iron (Fe)	Kojundo Chemical Laboratory Co., Ltd.	CAS: 7439-89-6
Arsenic (As)	Furukawa Denshi Co., Ltd.	CAS: 7440-38-2

RESOURCE AVAILABILITY

Lead contact

Further information and requests for resources and reagents should be directed to and will be fulfilled by the Lead Contact, Akiyasu Yamamoto (akiyasu@cc.tuat.ac.jp).

Materials availability

This study did not generate new unique materials.

Data and code availability

There is no dataset or code associated with this work.

METHOD DETAILS

Sample preparation

K-doped Ba122 polycrystalline bulk samples with a diameter of 10 mm and a thickness of ∼1.3 mm were synthesized via SPS using a mechanically alloyed powder. Elemental metals, namely, Ba (chunk, 99.9%), K (chunk, 98.0%), Fe (100 mesh, 99.9+%), and As (granule, 99.9999%), were weighed at a molar ratio of Ba:K:Fe:As = 0.6:0.4:2:2 in an Ar glove box. These metals were ground and mixed in a planetary ball-mill apparatus (Premium line P-7, Fritsch) to produce a mechanically alloyed K-doped Ba122 powder with a ball-mill energy of 200 MJ/kg (Häßler et al., 2013; Tokuta et al., 2020; Tokuta and Yamamoto, 2019). The powder was filled into a graphite SPS mold with an inner diameter of 10 mm. The temperature was then increased to 500°C, 550°C, 600°C, 650°C, 700°C, and 900°C at a rate of +50°C/min under a uniaxial pressure of 50 MPa using an SPS apparatus (LABOX-315R, SINTER LAND). After sintering at each temperature for 5 min, the pressure was removed and the samples were cooled to room temperature. For reference, a pellet composed of the same powder was vacuum-sealed in a quartz tube and sintered at 500°C for 48 h to obtain a bulk sample under ambient pressure.

Evaluations

An image of a disk-shaped bulk sample is shown in the inset of Figure 1. The density was calculated using the diameter, thickness, and mass of the sample, and the phase composition and structural properties were evaluated using X-ray diffraction (XRD) measurements (D2 PHASER 2nd Generation, Bruker) with Cu-K_α radiation at λ = 1.5418 Å. The lattice parameters a and c were calculated using the Rietveld refinement (DIFFRAC.TOPAS). The polished cross-sectional surfaces of the samples were used to observe the microstructure using scanning electron microscopy (SEM; S-3400N, Hitachi High-Tech Corporation) and scanning transmission electron microscopy (STEM; ARM200F, JEOL). Moreover, elemental analysis was performed using energy dispersive X-ray spectroscopy (EDX). Electrical resistivity measurements were performed between 20 K and 300 K using the conventional four-probe method for the samples cut into ∼0.5 × 1.2 × 5.0 mm^3, and magnetization measurements were conducted between up to 7 T using SQUID VSM (MPMS3, Quantum Design) for the samples cut into ∼0.5 × 1.2 × 2.8 mm^3. T_c was defined by 90% of the superconducting transition of the electrical resistivity, and the zero resistance temperature (T_c^{zero}) was defined as the temperature at which the resistivity reached 1 μΩ cm, which was close to the measurement limit. J_c was calculated using the magnetic hysteresis loop by employing the extended Bean's model.